Schweizerischer Erdbebendienst
Service Sismologique Suisse
Servizio Sismico Svizzero
Servizi da Terratrembels Svizzer

ETH
Eidgenössische Technische Hochschule Zürich
Swiss Federal Institute of Technology Zurich

# Buchs - Hochschule (SBUH)

## SITE CHARACTERIZATION REPORT

**Clotaire MICHEL, Carlo CAUZZI, Daniel ROTEN,**

**Valerio POGGI, Jan BURJANEK, Donat FÄH**


Sonneggstrasse 5 CH-8092 Zürich Switzerland; E-mail: clotaire.michel@sed.ethz.ch

Last modified : November 5, 2013

# Abstract

Ambient vibration array measurements were performed in the centre of the Rhine basin in Buchs. The new station SBUH of the Swiss Strong Motion Network located in the Northern part of Buchs city, close to the NTB school, is replacing the dial-up station SBUG. In order to characterize the velocity profile under the station, single station and array measurements with a $480\,\mathrm{m}$ aperture were performed. The H/V survey and polarization analysis showed that the Rhine basin in Buchs behave in a 1D fashion with a fundamental frequency around $0.6\,\mathrm{Hz}$ at the station site. The $12$ first meters correspond to sand with velocities around $300\,\mathrm{m/s}$. Below, a stiff layer with poorly constrained velocities ($450$ to $750\,\mathrm{m/s}$) corresponds to gravels down to approximately $30\,\mathrm{m}$ depth. At this depth, a velocity inversion is found, with velocities of the lower layer as low as $230\,\mathrm{m/s}$ increasing up to $600\,\mathrm{m/s}$ down to the bedrock at about $250\,\mathrm{m}$ depth. $V_{s,30}$ is found to be close to $420\,\mathrm{m/s}$, associated here to the ground types B and C, respectively for EC8 and SIA261 design codes. The theoretical SH transfer function and impedance contrast of the quarter-wavelength velocity computed from the inverted profiles support a large amplification at the resonance frequencies. Recordings on the new station will allow to validate the proposed 1D models.

# Contents

# 1 Introduction

The station SBUH (Buchs Hochschule) is part of the Swiss Strong Motion Network (SSMNet) in the Rhine valley. SBUH has been installed in the framework of the SSMNet Renewal project in 2012, in order to replace dial-up station SBUG, located 600 m to the West. This project includes also the site characterization. Passive array measurements have been selected as a standard tool to investigate these sites. A measurement campaign was therefore carried out on 14th September 2012 in the area of the NTB school in Buchs (Fig. 1), in order to characterize the soil column under SBUH station. According to the geological map, this station is located on the loose alluvia of Rhine river. Moreover, single station measurements in several points were already available in the city (see also the report on SBUA2 station). This report presents available boreholes around the station, the measurement setup, the results of the H/V analysis and of the array processing of the surface waves (dispersion curves). Then, an inversion of these results for velocity profiles is performed. Standard parameters are derived to evaluate the amplification at this site.

| Canton | City | Location | Station code | Site type | Slope |
|---|---|---|---|---|---|
| St Gallen | Buchs | Hochschule | SBUH | Deep sediments | Flat |

Table 1: Main characteristics of the study-site.


Figure 1: Picture of the site.

# 2 Boreholes

Boreholes are available in the region through the Office for Environment of canton St Gallen but they are relatively shallow. The closest to the station is displayed on Fig. 2 (see Fig. 3 for the exact location). It shows first that the ground water table was located at $2\,\mathrm{m}$ depth in 1968. Second, down to $11.85\,\mathrm{m}$, it shows mostly sand, and, below, a layer of gravels.

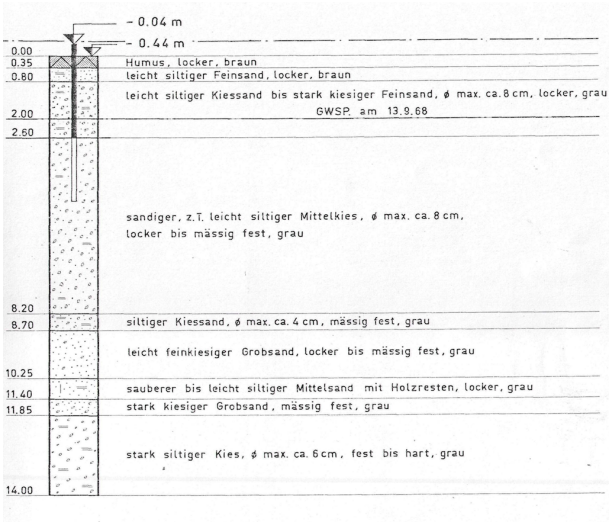


Figure 2: Closest available borehole to station SBUH (Amt für Umwelt Kanton St Gallen).

# 3 Experiment description

## 3.1 Ambient Vibrations

The ground surface is permanently subjected to ambient vibrations due to:

- natural sources (ocean and large-scale atmospheric phenomena) below $1\,\mathrm{Hz}$,
- local meteorological conditions (wind and rain) at frequencies around $1\,\mathrm{Hz}$ ,
- human activities (industrial machines, traffic…) at frequencies above $1\,\mathrm{Hz}$ [Bonnefoy-Claudet et al., 2006].

The objective of the measurements is to record these ambient vibrations and to use their propagation properties to infer the underground structure. First, the polarization of the recorded waves (H/V ratio) is used to derive the resonance frequencies of the soil column. Second, the arrival time delays at many different stations are used to derive the velocity of surface waves at different frequencies (dispersion). The information (H/V, dispersion curves) is then used to derive the properties of the soil column using an inversion procedure.

## 3.2 Equipment

For the array measurements, 12 Quanterra Q330 dataloggers named NR01 to NR12 and 14 Lennartz 3C 5 s seismometers were available (see Tab. 2). Each datalogger can record on 2 ports A (channels EH1, EH2, EH3 for Z, N, E directions) and B (channels EH4, EH5, EH6 for Z, N, E directions). Time synchronization was ensured by GPS. The sensors were placed on a metal tripod in a $20\,\mathrm{cm}$ deep hole, when possible, for better coupling with the ground.

| **Digitizer** | **Model** | **Number** | **Resolution** |
|---|---|---|---|
| | Quanterra Q330 | 12 | $24\,\mathrm{bits}$ |
| **Sensor type** | **Model** | **Number** | **Cut-off frequency** |
| Velocimeter | Lennartz 3C | 14 | $0.2\,\mathrm{Hz}$ |

Table 2: Equipment used.

## 3.3 Geometry of the arrays

Two array configurations were used, for a total of 5 rings of $10$, $25$, $50$, $120$ and $240\,\mathrm{m}$ radius around a central station. The first configuration includes the 3 inner rings with 14 sensors; the second configuration includes the 2 outer rings (plus the inner ring and the central station) with 14 sensors. The minimum inter-station distance and the aperture are therefore $10$ and $100\,\mathrm{m}$ and $10$ and $480\,\mathrm{m}$, respectively. The experimental setup is displayed in Fig. 3. The final usable datasets are detailed in section 4.2.

## 3.4 Positioning of the stations

For the array data, the sensor coordinates were measured using a differential GPS device (Leica Viva), including only a rover station and using the Real Time Kinematic technique provided by Swisstopo. It allows an absolute positioning with an accuracy of about $5\,\mathrm{cm}$ on the Swissgrid. However, for points BUH401 and BUH405 the precision was only $24$ and $19\,\mathrm{cm}$, respectively, due to the presence of trees.

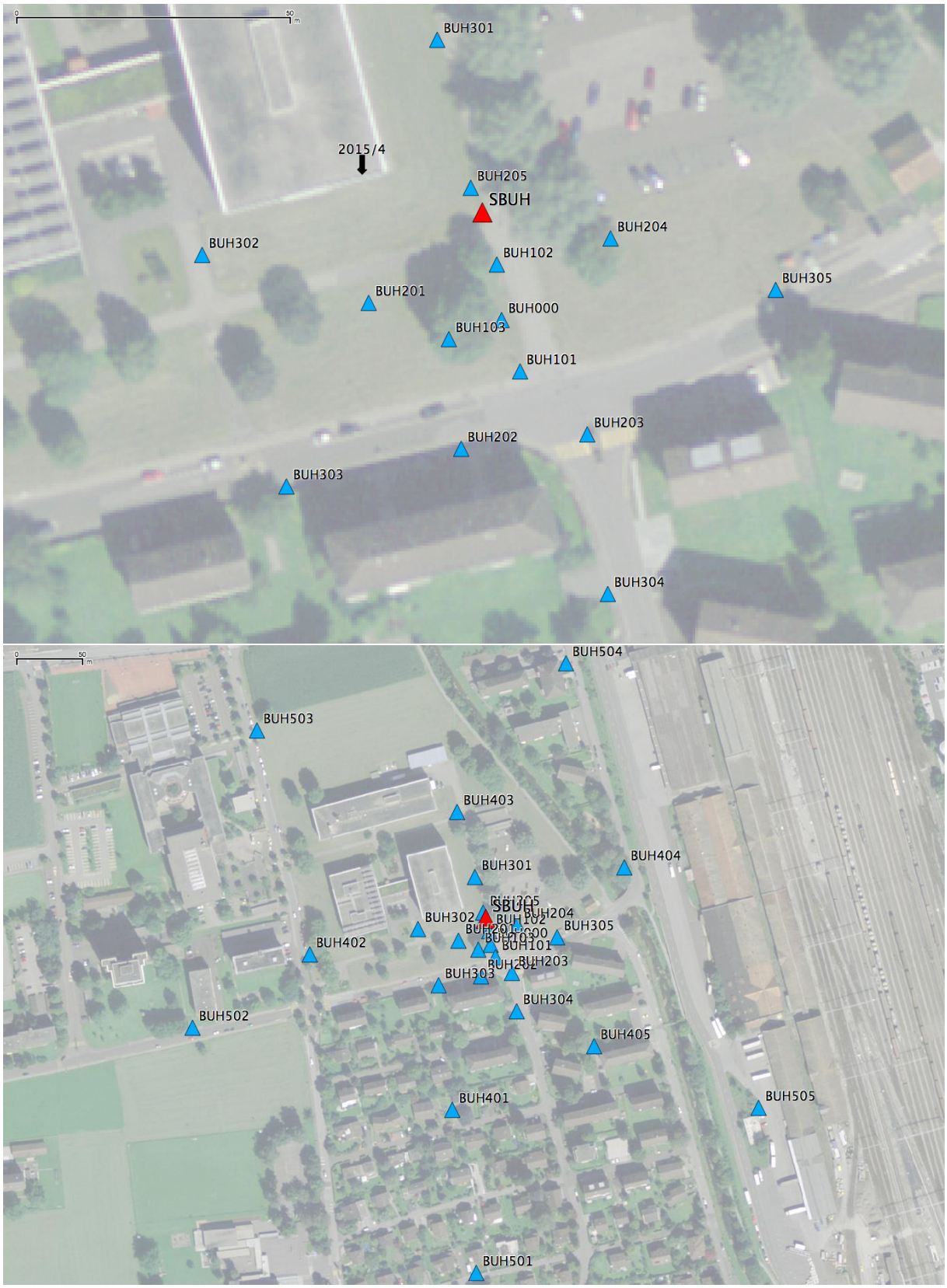


Figure 3: Geometry of the arrays: zoom on the first configuration, including the borehole 2015/4 presented on Fig. 2 (top) and view of the whole experiment (bottom).

# 4 Data quality

## 4.1 Usable data

The largest time windows were extracted, for which all the sensors of the array were in position and the GPS synchronization was ensured. Differential GPS measurements were not performed during the data acquisition during configuration 1 to avoid disturbances, but some took place during the acquisition of dataset 2. During these measurements, point BUH405 was touched at 12:30. Moreover, a military explosion occurred at 12:42, generating an air flow that shook some of the sensors. Peaks due to machines at $1.5$ and $2\,\mathrm{Hz}$ can be noticed on all recordings.

Orientation of the sensors was checked by maximizing the correlation with the central station at low frequencies [Poggi et al., 2012b]. Deviations lower than $7\,^\circ$ were found for all points. Original and rotated datasets are available for the 3C array analysis.

The characteristics of the datasets are detailed in Tab. 3.

## 4.2 Data processing

The data were first converted to SAC format including in the header the sensor coordinates (CH1903 system), the recording component and a name related to the position. The name is made of 3 letters characterizing the location (BUH here), 1 digit for the ring and 2 more digits for the number in the ring. Recordings were not corrected from the instrument response.

| Dataset | Starting Date | Time | Length | $F_s$ | Min. inter-distance | Aperture | # of points |
|---|---|---|---|---|---|---|---|
| 1 | 2012/09/14 | 8:38 | 117 min | 200 Hz | 10 m | 100 m | 14 |
| 2 | 2012/09/14 | 11:42 | 119 min | 200 Hz | 10 m | 480 m | 14 |

Table 3: Usable datasets.

# 5 H/V processing

## 5.1 Processing method and parameters

In order to process the H/V spectral ratios, several codes and methods were used. The classical H/V method was applied using the Geopsy `http://www.geopsy.org` software. In this method, the ratios of the smoothed Fourier Transform of selected time windows are averaged. Tukey windows (cosine taper of 5% width) of $100\,\mathrm{s}$ long overlapping by 50% were selected. Konno and Ohmachi [1998] smoothing procedure with b=60 was used. The classical H/V method of Fäh et al. [2001] was also applied.

Moreover, the time-frequency analysis method [Fäh et al., 2009] was used to estimate the ellipticity function more accurately using the Matlab code of V. Poggi. In this method, the time-frequency analysis using the Wavelet transform is computed for each component. For each frequency, the maxima over time (10 per minute with at least $0.1\,\mathrm{s}$ between each) in the TFA are determined. The Horizontal to Vertical ratio of amplitudes for each maxima is then computed and statistical properties for each frequency are derived. Cosine wavelet with parameter 9 was used. The mean of the distribution for each frequency is stored. For the sake of comparison, the time-frequency analysis of Fäh et al. [2001], based on the spectrogram, was also used, as well as the wavelet-based TFA coded in Geopsy.

The ellipticity extraction using the Capon analysis [Poggi and Fäh, 2010] on the array measurement was also performed (see section 6).

| Method | Freq. band | Win. length | Anti-trig. | Overlap | Smoothing |
|---|---|---|---|---|---|
| Standard H/V Geopsy | $0.2 - 20\,\mathrm{Hz}$ | $100\,\mathrm{s}$ | No | 50% | K&O 60 |
| Standard H/V D. Fäh | $0.2 - 20\,\mathrm{Hz}$ | $30\,\mathrm{s}$ | No | 75% | - |
| H/V TFA Geopsy | $0.2 - 20\,\mathrm{Hz}$ | Morlet m=8 fi=1 | No | - | - |
| H/V TFA D. Fäh | $0.2 - 20\,\mathrm{Hz}$ | Specgram | No | - | - |
| H/V TFA V. Poggi | $0.2 - 20\,\mathrm{Hz}$ | Cosine wpar=9 | No | - | No |

Table 4: Methods and parameters used for the H/V processing.

## 5.2 Results in the array

H/V curves are similar for all the recordings in the array (Fig. 4), showing the homogeneity of the site with a fundamental frequency around $0.6\,\mathrm{Hz}$ (Fig. 5). The fundamental frequency at the dial-up station SBUG is slightly lower ($0.5\,\mathrm{Hz}$). Moreover, all the methods to compute H/V ratios are compared on Fig. 6, where the classical methods were divided by $\sqrt{2}$ to correct from Love waves influence [Fäh et al., 2001]. The matching is good considering the parametrization of the codes of D. Fäh were kept with default values and not adapted to low frequency peaks. The 3C FK analysis provides similar results but is not able to explore the part related to the fundamental frequency due to the too small array aperture compared to the basin depth. The peak is clear at $0.61\,\mathrm{Hz}$, with a peak amplitude around 6.

Considering the shape of the deep Rhine basin, a 2D resonance could occur [Roten et al., 2006]. Polarization analysis on the array data was performed using the method of Burjánek

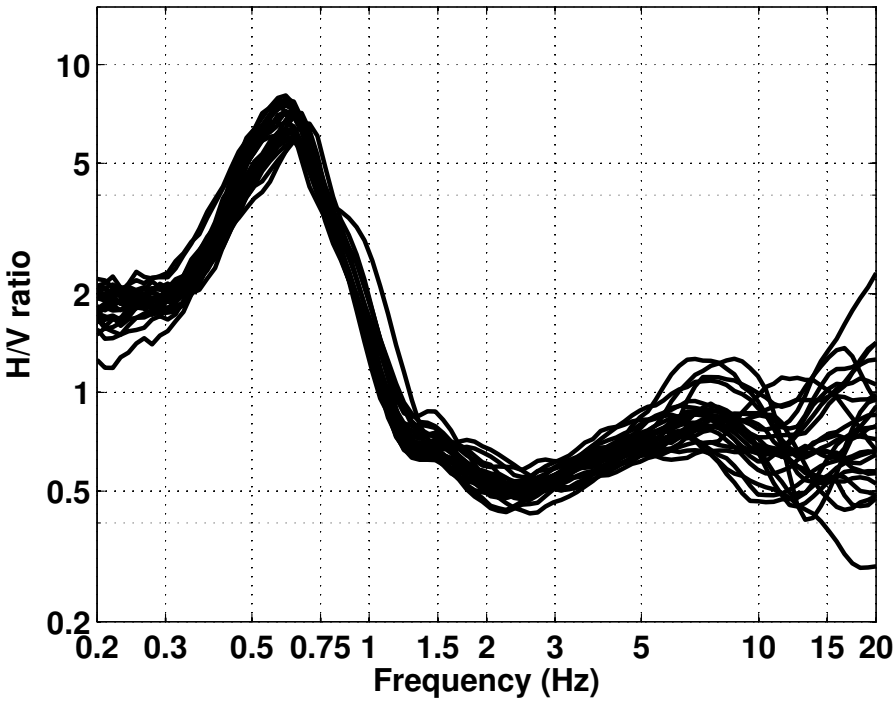


Figure 4: H/V spectral ratios (time-frequency analysis code V. Poggi).

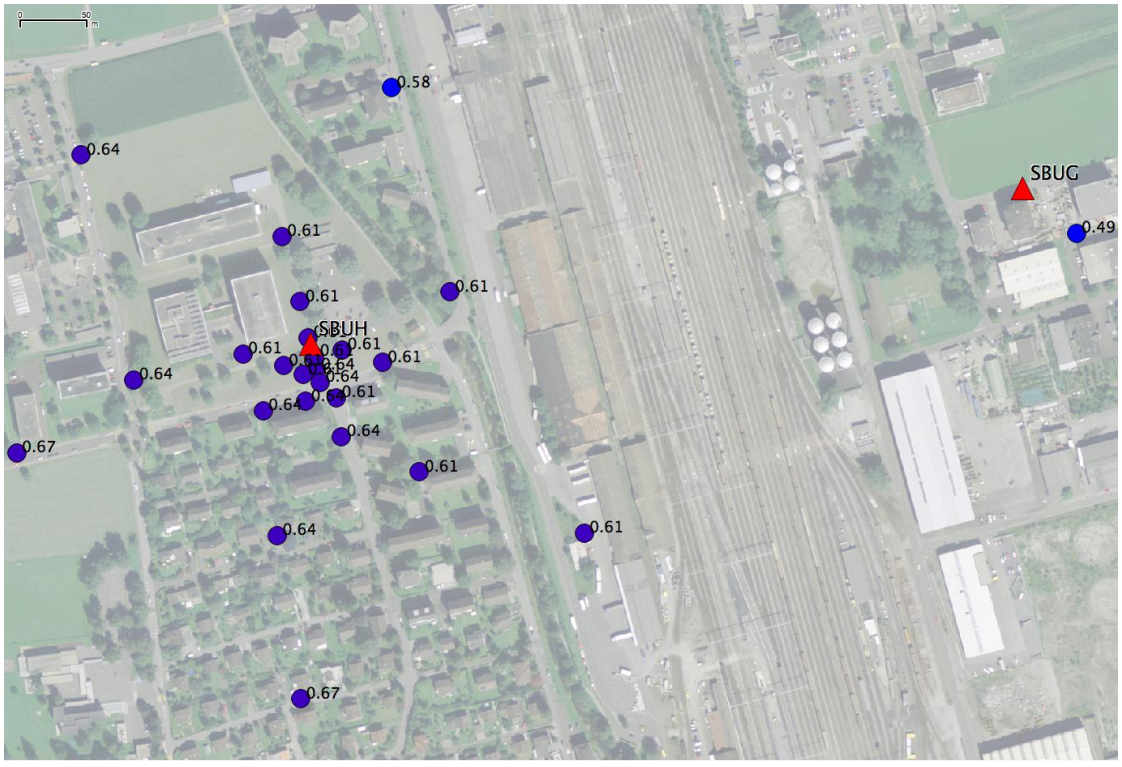


Figure 5: Fundamental frequencies in the array.

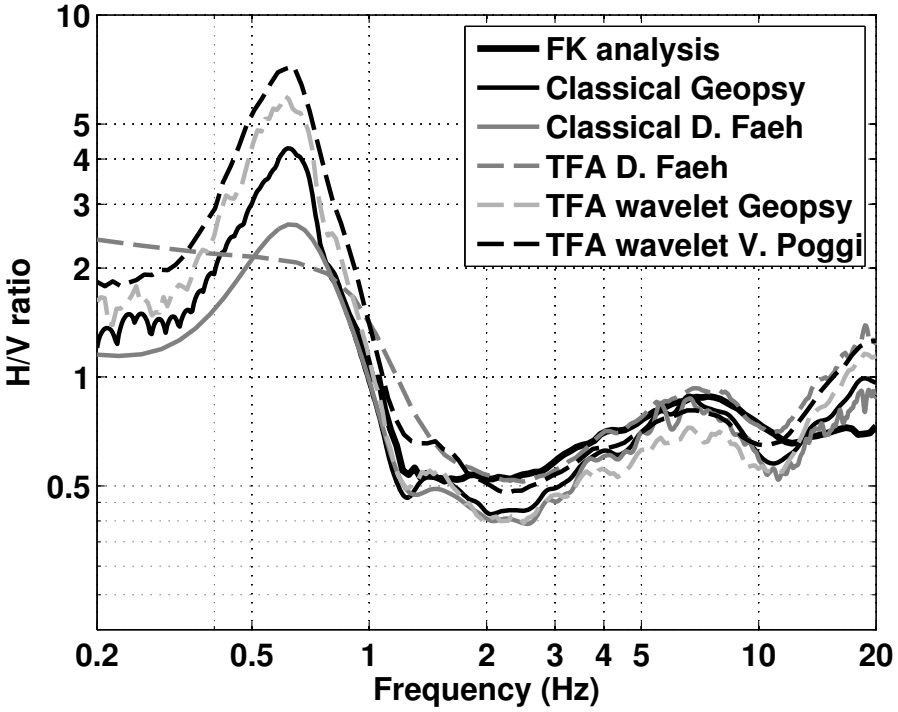


Figure 6: H/V spectral ratios for point BUH000 using the different codes. Classical methods were divided by $\sqrt{2}$.

et al. [2010]. For all points (e.g. in the array centre Fig. 7), the H/V peak is well recognized at $0.6\,\mathrm{Hz}$ but no preferred directionality is found. There is therefore no 2D resonance in this case, which is confirmed by the variation of the H/V peak observed across the valley (see next section).

## 5.3 Results in the whole city

Other H/V points are available in the city of Buchs (see also SBUA2 report). The results are displayed on Fig. 8. The values in the cross-sections show the decrease of the fundamental frequency from the edge to the valley centre. The station SBUG is nearly located on the deepest part of the basin and is representative for the city of Buchs.

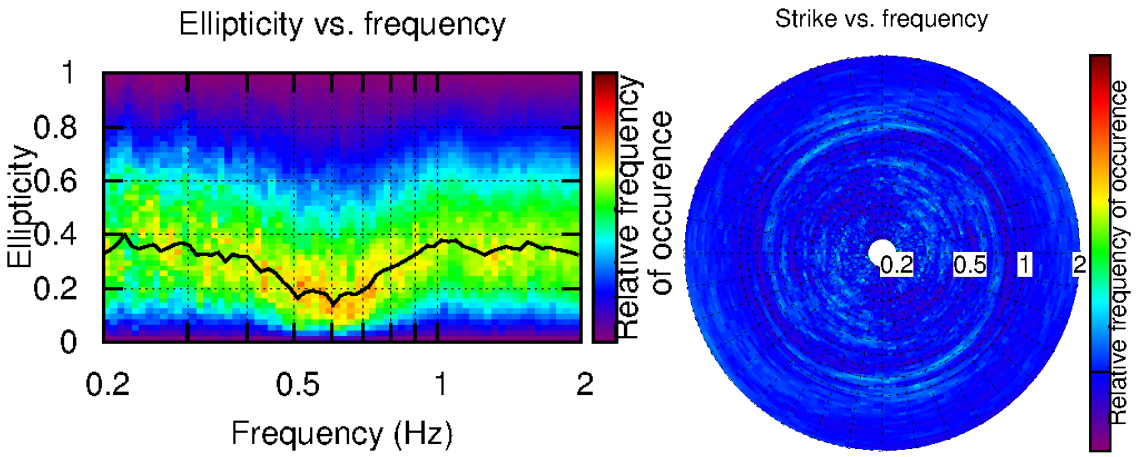


Figure 7: Polarization analysis at point BUH000. Left: Ellipticity (A trough in the ellipticity corresponds to horizontally polarized motion). Right: Strike of the polarization.

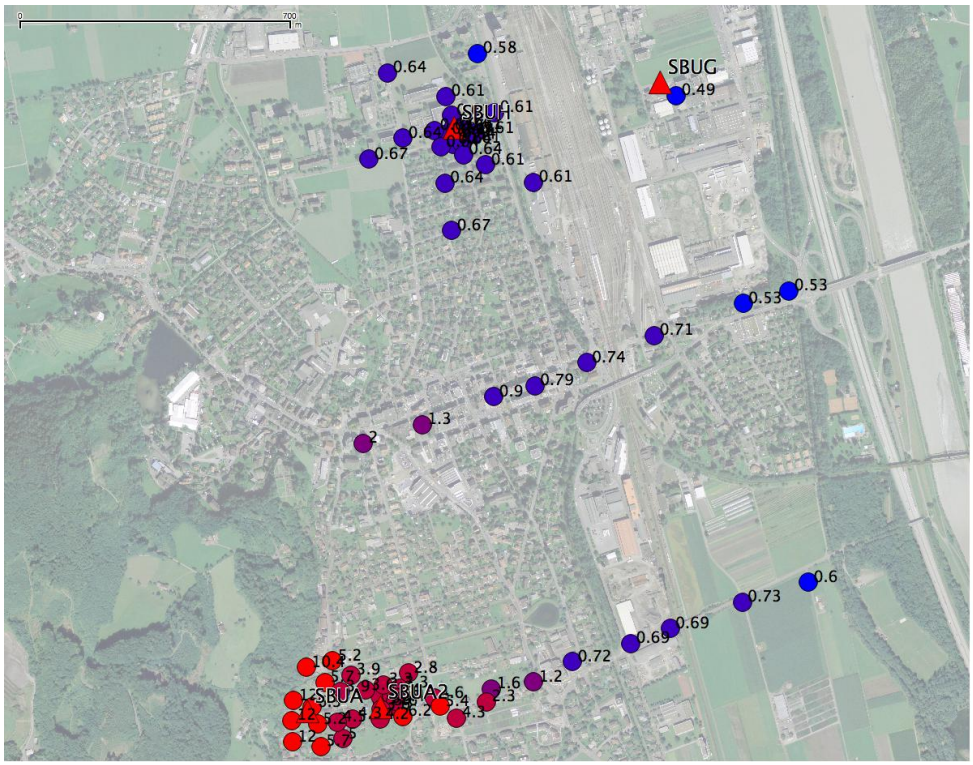


Figure 8: Fundamental frequencies in the city of Buchs.

# 6 Array processing

## 6.1 Processing methods and parameters

The vertical components of the arrays were processed using the High-resolution FK analysis [Capon, 1969] using the Geopsy `http://www.geopsy.org` software. Better results were obtained using large time windows (300T, where T stands for period). The FK distributions were concatenated.

Moreover, a 3C array analysis [Fäh et al., 2008] was also performed using the array_tool_3C software [Poggi and Fäh, 2010]. The results of computations of both datasets were merged to estimate the dispersion curves. It allows to derive Rayleigh and Love fundamental modes.

| Method | Set | Freq. band | Win. length | Anti-trig. | Overlap | Grid step | Grid size | # max. |
|---|---|---|---|---|---|---|---|---|
| HRFK 1C | 1 | $0.5 - 20\,\mathrm{Hz}$ | $300T$ | No | 50% | 0.001 | 0.6 | 5 |
| HRFK 1C | 2 | $0.5 - 20\,\mathrm{Hz}$ | $300T$ | No | 50% | 0.001 | 0.6 | 5 |
| HRFK 3C | 1 | $0.6 - 20\,\mathrm{Hz}$ | Wav. 10 Tap. 0.2 | No | 50% | 150 m/s | 2500 m/s | 5 |
| HRFK 3C | 2 | $0.6 - 20\,\mathrm{Hz}$ | Wav. 10 Tap. 0.2 | No | 50% | 150 m/s | 2500 m/s | 5 |

Table 5: Methods and parameters used for the array processing.

## 6.2 Obtained dispersion curves

The fundamental and a higher Rayleigh modes could be picked in the 1C FK analysis including their standard deviation (Fig. 9). The fundamental mode was picked between $0.8$ and $17.3\,\mathrm{Hz}$. The velocities are ranging from $1350\,\mathrm{m/s}$ at $0.8\,\mathrm{Hz}$ down to $270\,\mathrm{m/s}$ at $17.3\,\mathrm{Hz}$. Based on the array size, the obtained dispersion curves are broadband.

Using the 3C analysis (Fig. 9), if the vertical direction provides the same results as the 1C analysis (Fig. 10), the radial component provides more information about Rayleigh higher modes. Even if they cannot be picked with precision, 3 higher modes can be recognized. The higher mode picked from the vertical component is therefore the third higher mode. In the transverse direction, modes jumping between fundamental and first higher Love modes can be seen: between $3$ and $4\,\mathrm{Hz}$, the fundamental mode is disappearing whereas the first higher is appearing. Moreover another higher Love mode is found, which may be the forth higher mode after tests in the inversion. Fig. 10 is summarizing the picked curves.

On Fig. 11, the obtained Rayleigh dispersion curve in this experiment is compared to the one obtained in the large "Rheintal array" in Grabs, further North in the Rhine basin. They are similar except that the Rheintal array was located in a slightly deeper part of the basin (downstream) and is therefore slightly shifted towards lower frequencies. Unfortunately, the curve is not available at high frequencies for comparison. The array limits show the limited benefit of using an extremely large array in this case.

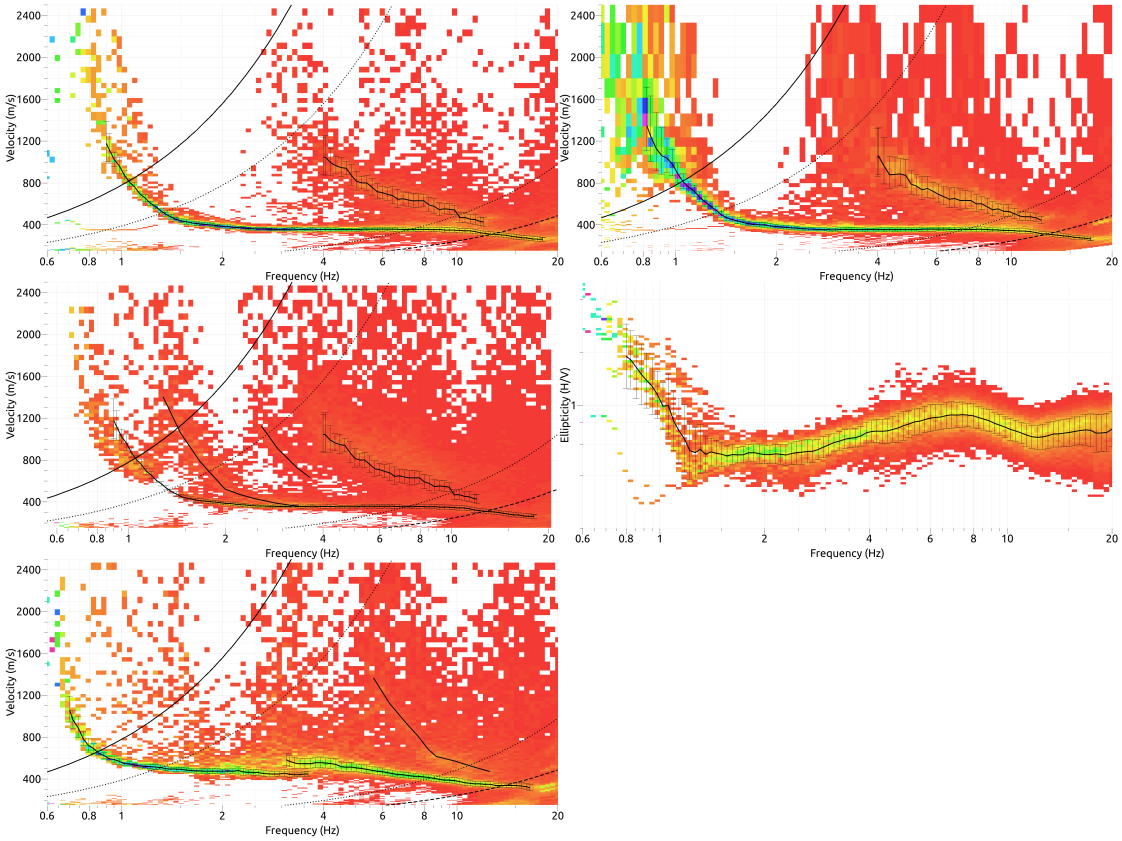


Figure 9: Dispersion curves and ellipticity obtained from the 1C (top right) and 3C array analysis (left and centre-right). Top: Vertical - Centre: Radial - Bottom: Transverse component.

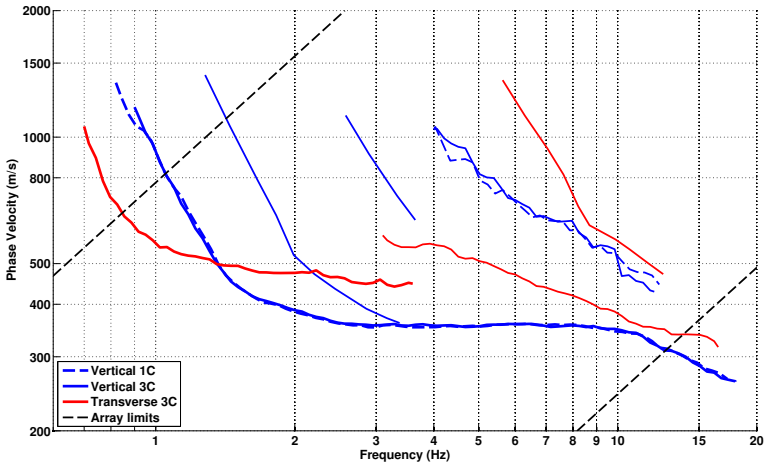


Figure 10: Picked dispersion curves from 1C and 3C analyses (thick lines for fundamental, thin lines for higher modes).

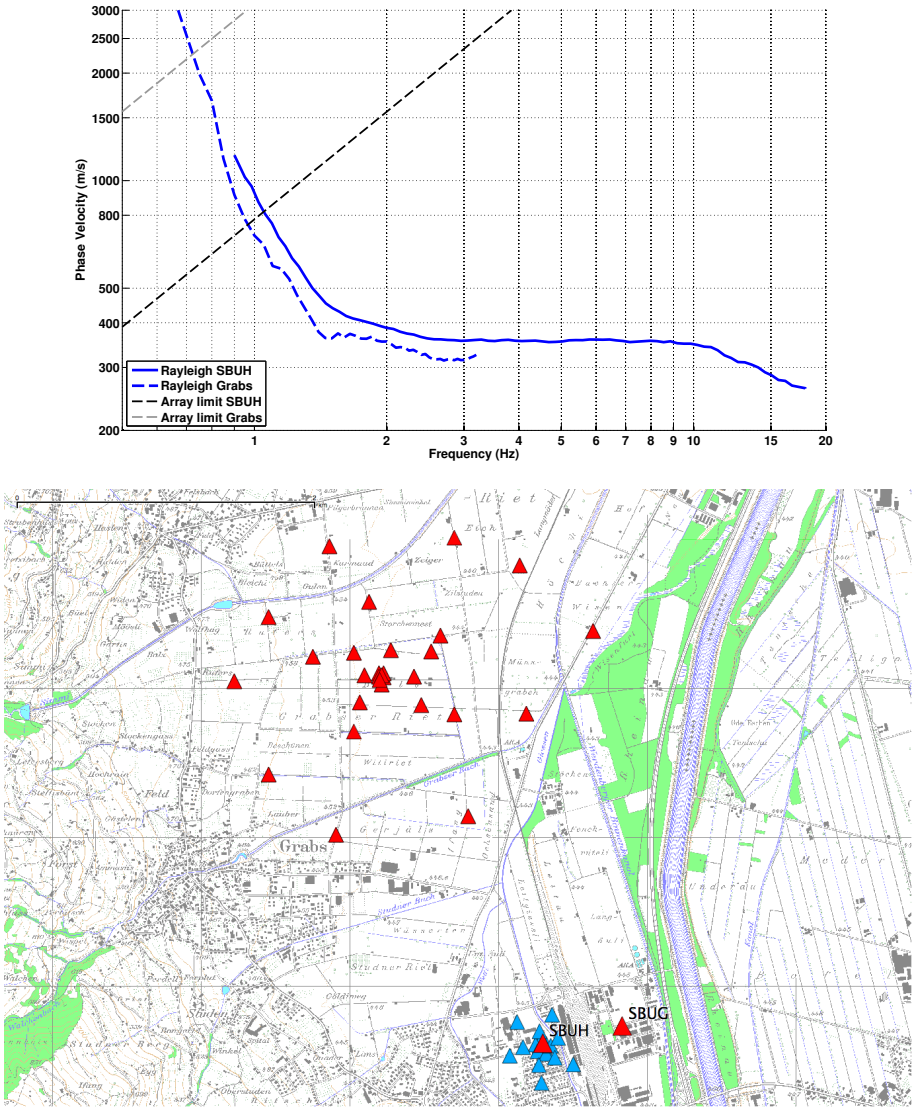


Figure 11: Top: Rayleigh dispersion curves of this experiment compared to the Rheintal experiment. Bottom: Location of the Rheintal experiment (red triangles) compared to the SBUH experiment (blue triangles).

# 7 Inversion and interpretation

## 7.1 Inversion

For the inversion, the Rayleigh fundamental and 3 first higher modes (3C analysis) and the Love fundamental and first higher modes dispersion curves within the array limits were used as simultaneous targets without standard deviation to avoid different weighting as well as the right flank of the ellipticity curve (code V. Poggi). A weight of 0.05 was assigned to the ellipticity curve and 0.05 to the ellipticity peak ($0.57\,\mathrm{Hz}$). All curves were resampled using 50 points between $0.5$ and $20\,\mathrm{Hz}$ in log scale.

The inversion was performed using the Improved Neighborhood Algorithm (NA) [Wathelet, 2008] implemented in the Dinver software. In this algorithm, the tuning parameters are the following: $Ns_0$ is the number of starting models, randomly distributed in the parameter space, $Nr$ is the the number of best cells considered around these $Ns_0$ models, $Ns$ is the number of new cells generated in the neighborhood of the $Nr$ cells ($Ns/Nr$ per cell) and $It_{max}$ is the number of iteration of this process. The process ends with $Ns_0 + Nr * \frac{Ns}{Nr} * It_{max}$ models. The used parameters are detailed in Tab. 6.

| $It_{max}$ | $Ns_0$ | $Ns$ | $Nr$ |
|---|---|---|---|
| 500 | 10000 | 100 | 100 |

Table 6: Tuning parameters of Neighborhood Algorithm.

During the inversion process, it happened that a low velocity zone is needed at about $30\,\mathrm{m}$ depth to fit the observed dispersion curves. For the other interfaces, velocity inversions were not allowed. The Poisson ratio was inverted in each layer in the range 0.2-0.4, up to 0.47 below the expected ground water table and the density was supposed equal to $2000\,\mathrm{kg/m^3}$ except for the layers assumed to be rock ($2500\,\mathrm{kg/m^3}$). Inversions with free layer depths as well as fixed layer depths were performed. 5 layers are enough to explain most of the targets (dispersion and ellipticity), but more layers are used to smooth the obtained results and better explore the parameter space. 5 independent runs of 5 different parametrization schemes (6 and 7 layers over a half space and 9, 11 and 13 layers with fixed depth) were performed. For further elaborations, the best models of these 25 runs were selected (Fig. 14).

The velocity profile is clearly layered. The $12$ first meters correspond to sand with velocities around $300\,\mathrm{m/s}$ (Fig. 2). Below, a stiff layer with poorly constrained velocities ($450$ to $750\,\mathrm{m/s}$) corresponds to gravels (Fig. 2). This layer extends down to approximately $30\,\mathrm{m}$ depth where a velocity inversion is found. The velocity is found as low as $230\,\mathrm{m/s}$ but increases rapidly in the next $10\,\mathrm{m}$ to about $400\,\mathrm{m/s}$. Another interface, poorly resolved, is found around $100\,\mathrm{m}$ depth where the velocity increases again to about $600\,\mathrm{m/s}$ down to the bedrock at about $250\,\mathrm{m}$ depth. The velocity in the bedrock is not constrained ($2500 - 3000\,\mathrm{m/s}$?).

When compared to the target curves (Fig. 12), the Love and Rayleigh modes, including the higher modes, as well as the right flank of the ellipticity and the ellipticity peak are well reproduced. It should be noticed that this level of matching cannot be reached without velocity inversion, but it also introduce large uncertainties in the final models.

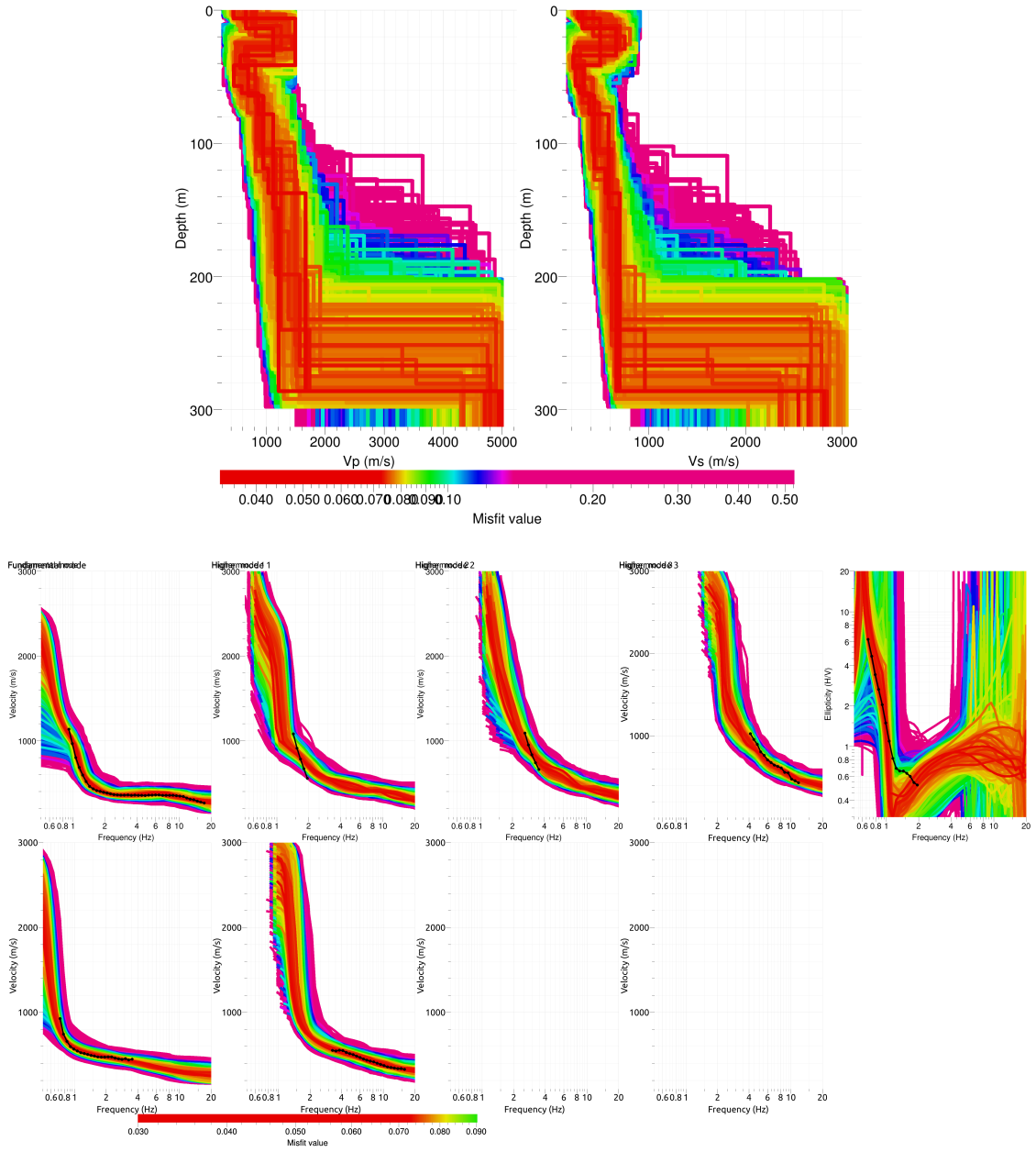


Figure 12: Inverted ground profiles in terms of $V_p$ and $V_s$ (top) and comparison between inverted models and measured Rayleigh and Love modes and corresponding ellipticity, free layer depth strategy.

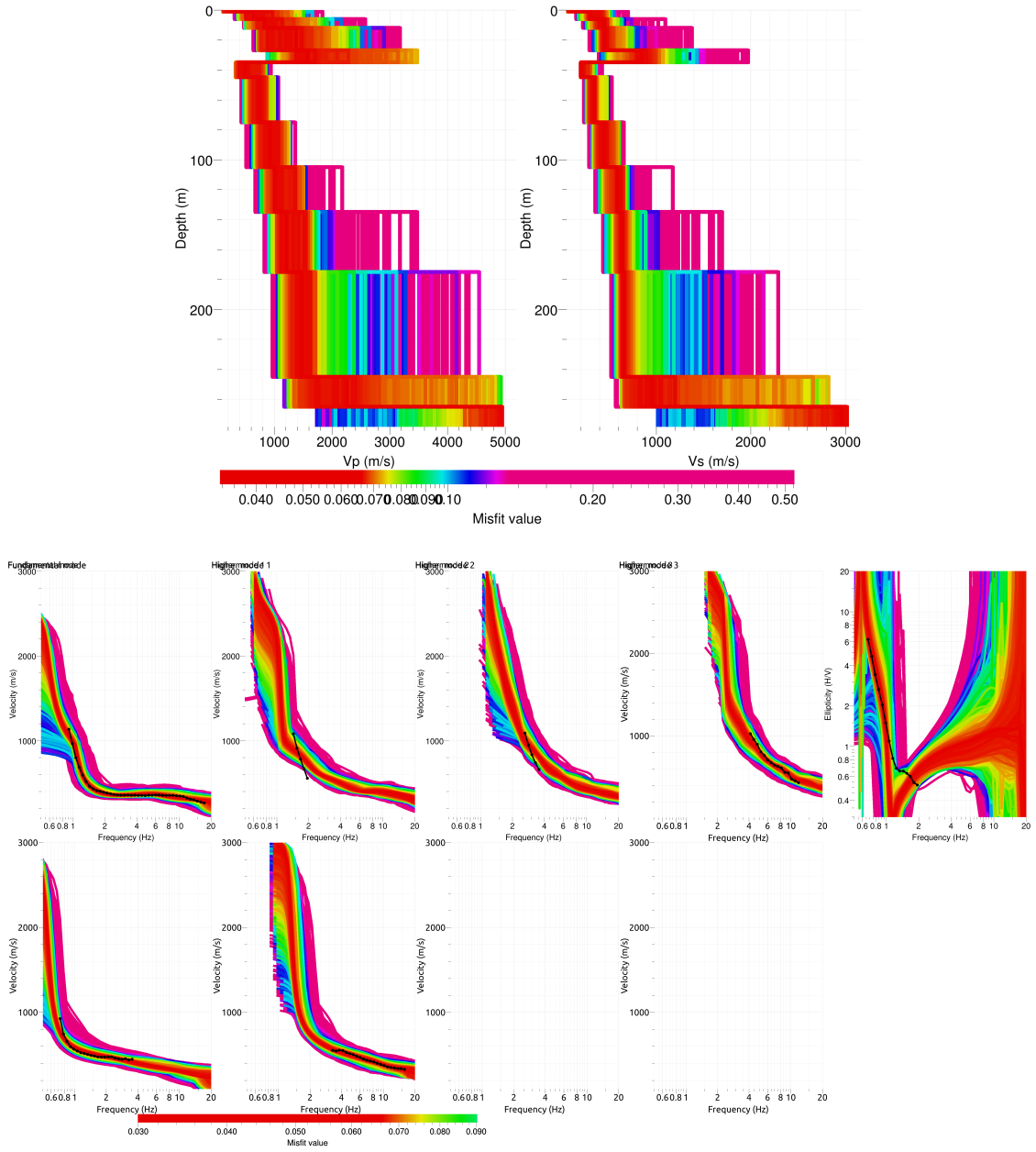


Figure 13: Inverted ground profiles in terms of $V_p$ and $V_s$ (top) and comparison between inverted models and measured Rayleigh and Love modes and corresponding ellipticity, fixed layer depth strategy.

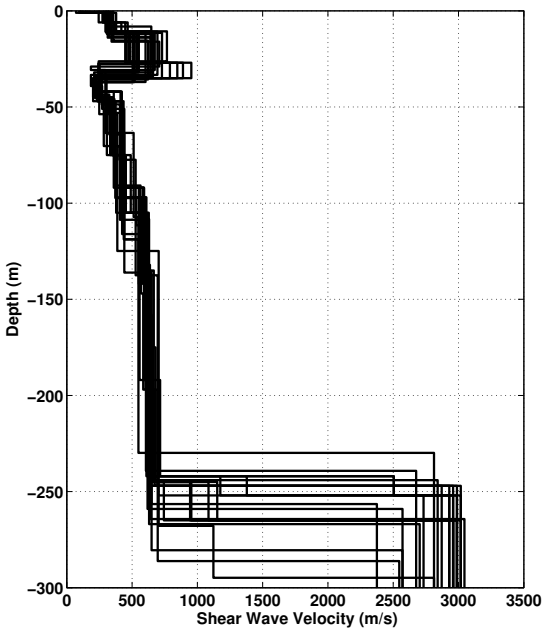


Figure 14: $V_s$ ground profiles for the selected 25 best models.

## 7.2 Travel time average velocities and ground type

The distribution of the travel time average velocities at different depths was computed from the selected models. The uncertainty, computed as the standard deviation of the distribution of travel time average velocities for the considered models, is also provided, but its meaning is doubtful since the parameter space was not fully explored. $V_{s,30}$ is found to be $420\,\mathrm{m/s}$, that is associated to type B in the Eurocode 8 [CEN, 2004] and C for SIA261 [SIA, 2003]. Both B and C could be argued for SIA261, but the most conservative is chosen here. This is in accordance with the ground type map of the Federal Office for Environment (`www.map.bafu.admin.ch`).

| | **Mean (m/s)** | **Uncertainty (m/s)** |
|---|---|---|
| $V_{s,5}$ | 276 | 43 |
| $V_{s,10}$ | 301 | 28 |
| $V_{s,20}$ | 375 | 32 |
| $V_{s,30}$ | 420 | 29 |
| $V_{s,40}$ | 385 | 21 |
| $V_{s,50}$ | 360 | 11 |
| $V_{s,100}$ | 380 | 12 |
| $V_{s,150}$ | 428 | 12 |
| $V_{s,200}$ | 465 | 8 |

Table 7: Travel time averages at different depths from the inverted models. Uncertainty is given as one standard deviation from the selected profiles.

## 7.3 SH transfer function and quarter-wavelength velocity

The quarter-wavelength velocity approach [Joyner et al., 1981] provides, for a given frequency, the average velocity at a depth corresponding to 1/4 of the wavelength of interest. It is useful to identify the frequency limits of the experimental data (ellipticity peak at $0.57\,\mathrm{Hz}$ and minimum frequency in dispersion curves at $0.85\,\mathrm{Hz}$ here). The results using this proxy show that the dispersion curves constrain the profiles down to $120\,\mathrm{m}$ and no data is controlling the results below $200\,\mathrm{m}$ (Fig. 15). Moreover, the quarter wavelength impedance-contrast introduced by Poggi et al. [2012a] is also displayed in the figure. It corresponds to the ratio between two quarter-wavelength average velocities, respectively from the top and the bottom part of the velocity profile, at a given frequency [Poggi et al., 2012a]. It shows a trough (inverse shows a peak) at the resonance frequency.
Moreover, the theoretical SH-wave transfer function for vertical propagation [Roesset, 1970] is computed from the inverted profiles. It is compared to the quarter-wavelength amplification [Joyner et al., 1981], that however cannot take resonances into account (Fig. 16). In this case, the models are predicting large amplifications at the resonance frequencies at $0.6$, $1.4$, $2.4$ and around $6.5\,\mathrm{Hz}$.

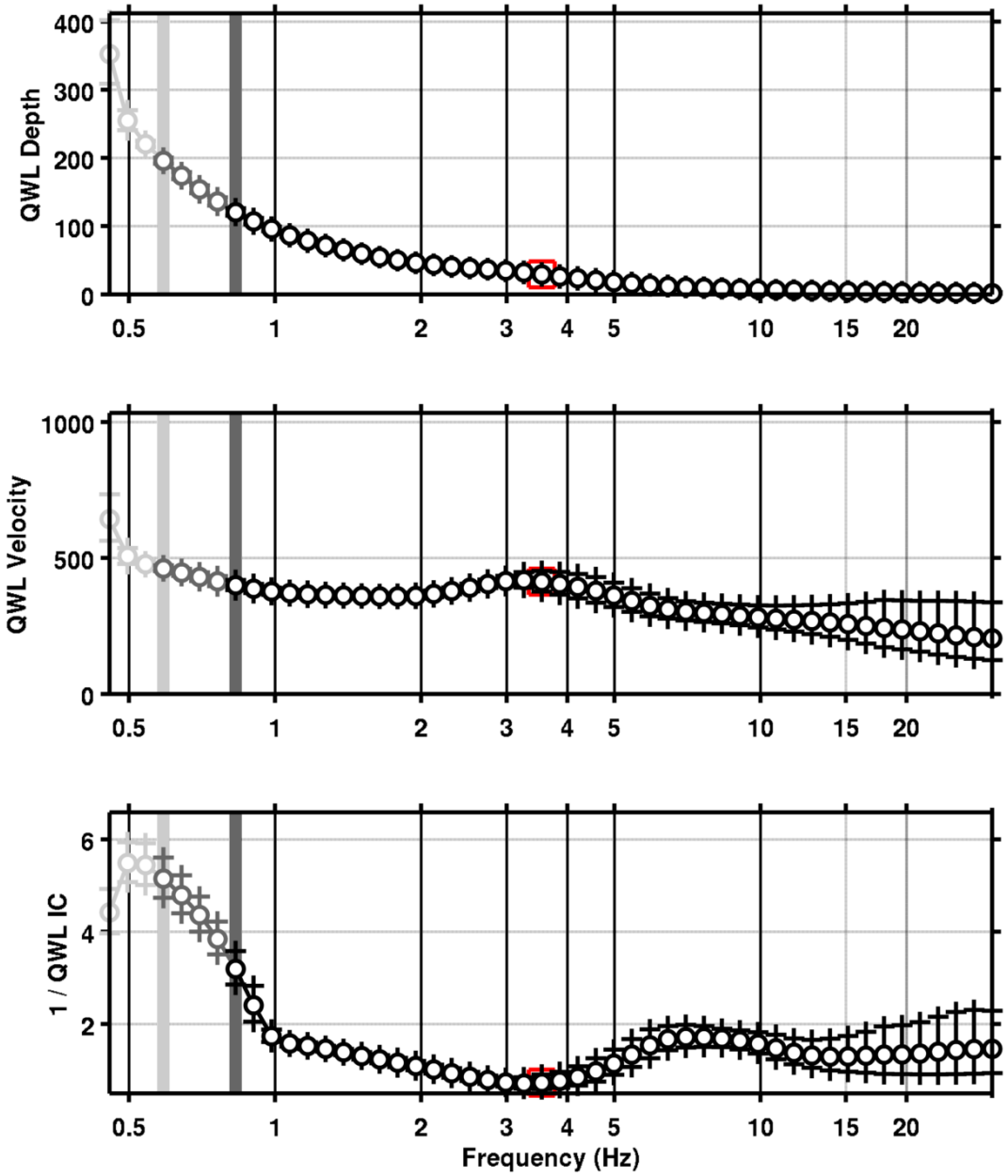


Figure 15: Quarter wavelength velocity representation of the velocity profile (top: depth, centre: velocity, bottom: inverse of the impedance contrast). Black curve is constrained by the dispersion curves, light grey is not constrained by the data. Red square is corresponding to $V_{s,30}$.

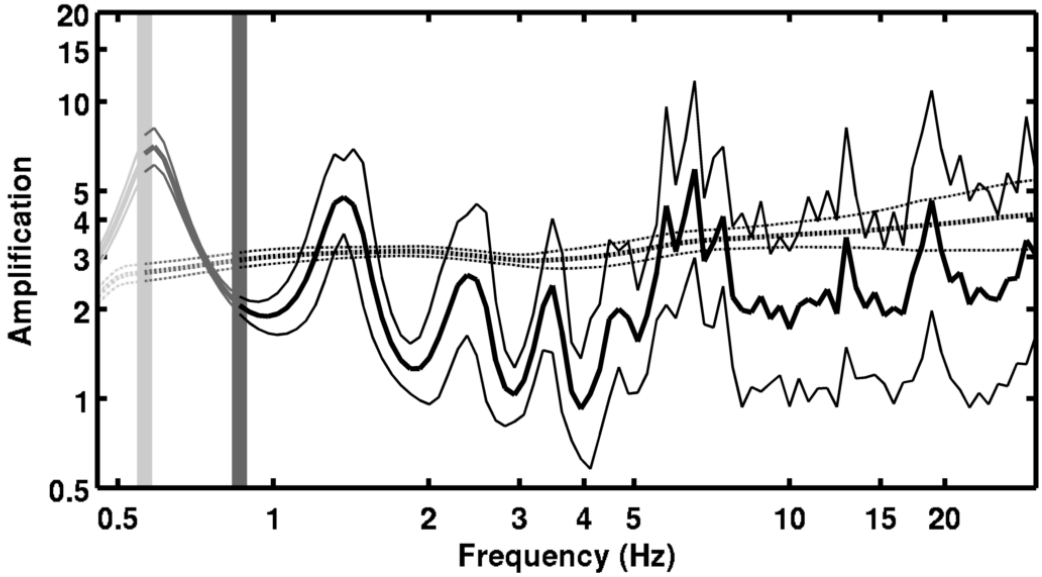


Figure 16: Theoretical SH transfer function (solid line) and quarter wavelength impedance contrast (dashed line) with their standard deviation. Significance of the greyshades is detailed in Fig. 15.

# 8 Conclusions

The array measurements presented in this study were successful in deriving a velocity model for the Hochschule site in Buchs, below the SBUH station. We found a layered velocity profile. The $12$ first meters correspond to sand with velocities around $300\,\mathrm{m/s}$. Below, a stiff layer with poorly constrained velocities ($450$ to $750\,\mathrm{m/s}$) corresponds to gravels down to approximately $30\,\mathrm{m}$ depth. At this depth, a velocity inversion is found, with velocities of the lower layer as low as $230\,\mathrm{m/s}$ increasing up to $600\,\mathrm{m/s}$ down to the bedrock at about $250\,\mathrm{m}$ depth. Moreover, the basin was found to resonate in a 1D mode at $0.6\,\mathrm{Hz}$ at the station site. $V_{s,30}$ is found to be close to $420\,\mathrm{m/s}$. The EC8 and SIA261 ground types are B and C, respectively. Recordings on the new station will allow to validate the proposed 1D models.

# Acknowledgements

The authors thank Nandan Shyam for the help during the array measurements and Beat Müller from the Office for Environment of the Canton St Gallen who provided the boreholes.

# References

Sylvette Bonnefoy-Claudet, Fabrice Cotton, and Pierre-Yves Bard. The nature of noise wavefield and its applications for site effects studies. *Earth-Science Reviews*, 79(3-4): 205–227, December 2006. ISSN 00128252. doi: 10.1016/j.earscirev.2006.07.004. URL http://linkinghub.elsevier.com/retrieve/pii/S0012825206001012.

Jan Burjánek, Gabriela Gassner-Stamm, Valerio Poggi, Jeffrey R. Moore, and Donat Fäh. Ambient vibration analysis of an unstable mountain slope. *Geophysical Journal International*, 180(2):820–828, February 2010. ISSN 0956540X. doi: 10.1111/j.1365-246X.2009.04451.x. URL http://doi.wiley.com/10.1111/j.1365-246X.2009.04451.x.

J. Capon. High-Resolution Frequency-Wavenumber Spectrum Analysis. *Proceedings of the IEEE*, 57(8):1408–1418, 1969.

CEN. *Eurocode 8: Design of structures for earthquake resistance - Part 1: General rules, seismic actions and rules for buildings*. European Committee for Standardization, en 1998-1: edition, 2004.

Donat Fäh, Fortunat Kind, and Domenico Giardini. A theoretical investigation of average H / V ratios. *Geophysical Journal International*, 145:535–549, 2001.

Donat Fäh, Gabriela Stamm, and Hans-Balder Havenith. Analysis of three-component ambient vibration array measurements. *Geophysical Journal International*, 172(1):199–213, January 2008. ISSN 0956540X. doi: 10.1111/j.1365-246X.2007.03625.x. URL http://doi.wiley.com/10.1111/j.1365-246X.2007.03625.x.

Donat Fäh, Marc Wathelet, Miriam Kristekova, Hans-Balder Havenith, Brigitte Endrun, Gabriela Stamm, Valerio Poggi, Jan Burjanek, and Cécile Cornou. Using Ellipticity Information for Site Characterisation Using Ellipticity Information for Site Characterisation. Technical report, NERIES JRA4 Task B2, 2009.

William B. Joyner, Richard E. Warrick, and Thomas E. Fumal. The effect of Quaternary alluvium on strong ground motion in the Coyote Lake, California, earthquake of 1979. *Bulletin of the Seismological Society of America*, 71(4):1333–1349, 1981.

Katsuaki Konno and Tatsuo Ohmachi. Ground-Motion Characteristics Estimated from Spectral Ratio between Horizontal and Vertical Components of Microtremor. *Bulletin of the Seismological Society of America*, 88(1):228–241, 1998.

Valerio Poggi and Donat Fäh. Estimating Rayleigh wave particle motion from three-component array analysis of ambient vibrations. *Geophysical Journal International*, 180(1):251–267, January 2010. ISSN 0956540X. doi: 10.1111/j.1365-246X.2009.04402.x. URL http://doi.wiley.com/10.1111/j.1365-246X.2009.04402.x.

Valerio Poggi, Benjamin Edwards, and Donat Fäh. Characterizing the Vertical-to-Horizontal Ratio of Ground Motion at Soft Sediment-Sites. *Bulletin of the Seismological Society of America*, 102(6), 2012a. doi: 10.1785/0120120039.

Valerio Poggi, Donat Fäh, Jan Burjanek, and Domenico Giardini. The use of Rayleigh-wave ellipticity for site-specific hazard assessment and microzonation: application to the city of Lucerne, Switzerland. *Geophysical Journal International*, 188(3):1154–1172, March 2012b. ISSN 0956540X. doi: 10.1111/j.1365-246X.2011.05305.x. URL `http://doi.wiley.com/10.1111/j.1365-246X.2011.05305.x`.

J.M. Roesset. Fundamentals of soil amplification. In R. J. Hansen, editor, *Seismic Design for Nuclear Power Plants*, pages 183–244. M.I.T. Press, Cambridge, Mass., 1970. ISBN 978-0-262-08041-5. URL `http://mitpress.mit.edu/catalog/item/default.asp?ttype=2\&tid=5998`.

Daniel Roten, Donat Fäh, Cécile Cornou, and Domenico Giardini. Two-dimensional resonances in Alpine valleys identified from ambient vibration wavefields. *Geophysical Journal International*, 165(3):889–905, June 2006. ISSN 0956540X. doi: 10.1111/j.1365-246X.2006.02935.x. URL `http://doi.wiley.com/10.1111/j.1365-246X.2006.02935.x`.

SIA. *SIA 261 Actions sur les structures porteuses*. Société suisse des ingénieurs et des architectes, Zürich, sia 261:20 edition, 2003.

Marc Wathelet. An improved neighborhood algorithm: Parameter conditions and dynamic scaling. *Geophysical Research Letters*, 35(9):1–5, May 2008. ISSN 0094-8276. doi: 10.1029/2008GL033256. URL `http://www.agu.org/pubs/crossref/2008/2008GL033256.shtml`.